Online-Journals.org

iJOE International Journal of Online and Biomedical Engineering

iJOE | eISSN: 2626-8493 | Vol. 22 No. 4 (2026) | OPEN ACCESS

https://doi.org/10.3991/ijoe.v22i04.59455

PAPER

Numerical Simulation-Based Design of a Pneumatic Finger Rehabilitation Robot for Tele-Rehabilitation

Dongze Li[1], **Kok Beng Gan**[1] (✉), **Kok Swee Sim**[2]

[1]Universiti Kebangsaan Malaysia, Selangor, Malaysia

[2]Multimedia University, Malacca, Malaysia

kbgan@ukm.edu.my

ABSTRACT

Hand motor function rehabilitation after stroke or traumatic injury requires repetitive, task-specific training, which is often limited by therapist availability and clinical resources. This study presents a lightweight, modular, and wearable pneumatic robotic arm for finger rehabilitation, designed to support tele-rehabilitation applications. The system employs a four-link mechanical structure that accommodates variations in finger length and enables natural flexion and extension without the need for individual customization. Motion control is achieved using a discrete-time proportional-integral-derivative (PID) controller with aerodynamic drag compensation, ensuring stable and accurate actuation under compressible air dynamics. A stage-specific pressure strategy is implemented, applying 0.1 MPa for early mobilization and 0.3 MPa for intensive training, enabling up to 80° of finger bending within 2.5 s. Network-induced latency and sensor delay are explicitly modeled in the control loop, and their effects on response time and tracking accuracy are evaluated through numerical simulations. Simulation results demonstrate a motion tracking error below 2°, with control errors remaining bounded under network latencies up to 50 ms, confirming real-time responsiveness suitable for remote rehabilitation scenarios. These findings support the feasibility of a scalable, cost-effective, and clinically viable pneumatic rehabilitation platform for individualized hand therapy and tele-rehabilitation deployment.

KEYWORDS

finger rehabilitation robot, pneumatic system modeling, wearable exoskeleton, motion simulation, adaptive control

1 INTRODUCTION

Robotic rehabilitation has advanced rapidly in recent years, extending robotic technologies into medical applications with promising outcomes. This study introduces a wearable finger rehabilitation robotic arm that mounts directly on the hand and employs pneumatic actuation to replicate physiological finger motion. The device is designed to assist patients with finger motor impairments in performing

Li, D., Gan, K. B., Sim, K. S. (2026). Numerical Simulation-Based Design of a Pneumatic Finger Rehabilitation Robot for Tele-Rehabilitation. *International Journal of Online and Biomedical Engineering (iJOE)*, 22(4), pp. 123–139. https://doi.org/10.3991/ijoe.v22i04.59455

Article submitted 2025-11-02. Revision uploaded 2026-01-06. Final acceptance 2026-01-06.

structured rehabilitation exercises independently [1]. Hand function is essential for daily activities and fine manipulation; however, it is highly susceptible to occupational injuries, which account for nearly one-quarter of workplace accidents. Such injuries often require prolonged rehabilitation and may still result in incomplete functional recovery [2]. These challenges underscore the need for effective, scalable, and patient-specific rehabilitation solutions [3].

Continuous Passive Motion (CPM), introduced by Salter in 1960, applies externally driven, repetitive joint motion to promote circulation, reduce stiffness, and accelerate recovery [4]. Although effective, CPM is highly repetitive and labor-intensive, placing significant demands on therapists [5]. To improve scalability and consistency, exoskeleton-based robotic systems have been developed to automate CPM-like therapy, delivering controlled and prolonged joint motion while reducing clinician workload [6]. These advances highlight the need for robotic devices specifically designed for finger rehabilitation [7]. Progress in bionic prosthetics and mechatronic miniaturization has further accelerated developments in rehabilitation robotics [8]. Early research in the 1990s produced prosthetic limbs that informed musculoskeletal kinematics and demonstrated functional restoration through biomimetic design [9]. With the advent of advanced materials, compact actuators, and integrated sensing and control technologies, the design of assistive mechanisms for finger joints has become both feasible and clinically relevant, reinforcing the importance of safety and reliability [10–11].

Commercial platforms, such as the Hand Mentor, integrate visual feedback with finger flexion units to guide patients through rehabilitation exercises, with the exoskeleton aiding as needed [12–13]. However, these systems constrain all fingers simultaneously, preventing targeted single-finger therapy and limiting individualized rehabilitation [14]. In contrast, recent research prototypes emphasize independent actuation of each finger joint, enabling more precise, patient-specific rehabilitation strategies.

Alternative architectures have been explored to overcome these limitations. A German design implemented joint-level actuation using two links with independent drives per joint and integrated angle sensors for real-time feedback [15]. However, the large number of actuators increased system complexity, reduced multi-finger training efficiency, and limited adaptability to different finger lengths [16]. Japanese groups developed high-degree-of-freedom systems incorporating wrist and palm actuation, but their size and complexity restricted portability and clinical applicability [17–18]. In China, research has accelerated with strong institutional investment. For instance, the Harbin Institute of Technology proposed a motor-driven four-bar mechanism with integrated joint sensors for adaptive force control [19]; however, its fixed configuration limited adaptability to inter-patient variability in hand anatomy [20–21]. At Huazhong University of Science and Technology, researchers investigated smart materials such as shape memory alloys and tendon-like transmissions to emulate finger flexor-extensor functions with compliant actuation [22–24]. While these approaches improve biomimicry and safety, they face challenges related to actuator mass, output stability, and wearability.

Collectively, prior research highlights a critical design trade-off: rehabilitation devices must balance motion fidelity, safety, portability, modularity for varying finger lengths, and control simplicity. To address these challenges, this study proposes a wearable, linkage-driven robotic arm that integrates pneumatic actuation with a modular design. Unlike motor-driven or shape-memory alloy systems, the proposed approach employs compressed air to drive a four-link mechanism that replicates finger flexion–extension. This strategy enhances safety and adaptability while providing a foundation for both simulation and experimental validation. The objective of this work is to

design and develop a lightweight, modular, pneumatic-driven 3D finger rehabilitation robotic arm model that supports individualized therapy, maintains control accuracy under network latency, and balances portability with clinical applicability.

2 METHODOLOGY

The design of the finger rehabilitation robotic arm was developed through a systematic three-dimensional (3D) modeling process. Individual components were first modeled to ensure structural accuracy, ergonomic suitability, and manufacturability. These components included the arm and thumb support structures, joint mechanisms comprising the first and second joints with their respective fixing blocks, and the strap system for finger and arm stabilization. After individual modeling, all components were integrated into a complete assembly to evaluate overall functionality, alignment, and design feasibility.

2.1 Design requirements

The proposed design encompasses the integration of four distinct components: parameterized modular joint structures with passive sliding grooves, which are engineered to adapt to finger lengths ranging from 60 to 110 mm; elastic hook-and-loop straps with three-point fixation, which are designed to accommodate finger diameters ranging from 15 to 30 mm; Collectively, these mechanisms ensure the device's compatibility with diverse patient hand anatomies while preserving motion accuracy and safety. The details of the design matrix are shown in Table 1 and ensures all design requirements for the pneumatic finger rehabilitation robot. It supports compliance during design reviews, simulations, and clinical validation.

Table 1. Design matrix for the finger rehabilitation robotic arm

Category	Requirement Description	Acceptance Criteria
Functional	Independent actuation for single-finger therapy	Device can actuate any single finger independently without affecting others
Functional	Four-link mechanism replicates MCP, PIP, DIP motion	Simulated vs measured angles deviate ≤ 2° across MCP/PIP/DIP
Functional	Stage-specific pressure modes: 0.1 MPa (early), 0.3 MPa (intensive)	0.1 MPa achieves ≥ 28° in 2.5 s; 0.3 MPa achieves ≈ 80° in 2.5 s
Performance	ROM thresholds vs pressure	≥ 28° @0.1 MPa; ≈ 48° @0.2 MPa; ≈ 80° @0.3 MPa within 2.5 s
Performance	Control accuracy ≤ 2° under nominal conditions	Mean absolute error ≤ 2°; peak ≤ 3° during cycles
Performance	Latency ≤ 50 ms; response time ≤ 2.7 s; error ≤ 3.8°	At ≤ 50 ms latency, response time ≤ 2.7 s and control error ≤ 3.8°
Mechanical	Arm support: high-strength aluminium alloy	Material certificate verifies alloy grade and strength; mass within design spec
Mechanical	Copper pins and self-lubricating sleeves to reduce wear	After 1×10^5, wear within limits; pins/sleeves replaceable < 10 min
Safety	Diffuse-reflective strap interlocks block activation if unfastened	With strap open, system remains inhibited and logs event

(Continued)

Table 1. Design matrix for the finger rehabilitation robotic arm *(Continued)*

Category	Requirement Description	Acceptance Criteria
Safety	Pressure capped at 0.3 MPa; fail-safe vent on fault	Commands above 0.3 MPa rejected; on fault, vent-to-safe executed within 500 ms
Tele-Rehab Control	Predictive control to compensate latency	Controller maintains ROM targets and accuracy under injected delays
Maintainability	Pins/bushings easily replaceable; bolted modular joints	Replacement possible with basic tools; module swap < 15 min

2.2 Three-dimensional modeling of arm support

The arm support plate was modeled using statistical data of average human hand dimensions as the design reference to ensure ergonomic suitability. Its primary function is to stabilize the patient's forearm and provide an interface for other components of the finger rehabilitation mechanism. High-strength aluminum alloy was selected as the construction material to guarantee durability, structural rigidity, and long-term reliability while maintaining an ergonomic and aesthetically refined design. In addition to supporting the forearm during therapy, the arm support serves as the mounting base for all other modules. As shown in Figure 1, the arm support establishes the global reference frame for kinematic reconstruction and defines load paths to the fixture.

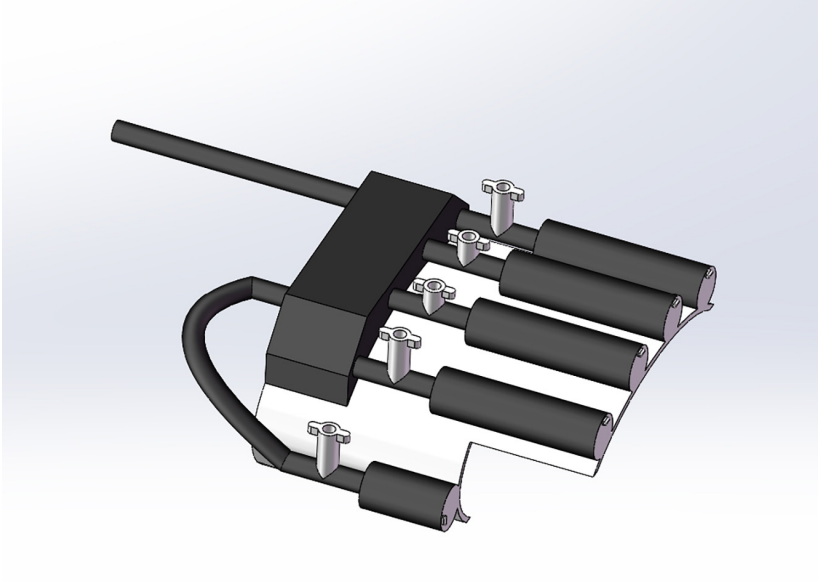

Fig. 1. Three-dimensional modelling of arm support

2.3 Three-dimensional modeling of arm and assembly

The thumb support block serves as the mounting base for the thumb actuator and is connected via a rotating pin. The pin is fabricated from copper, which is softer than the surrounding high-strength aluminum alloy structure. This material selection localizes wear to the pin, minimizing damage to major components during long-term rotational motion. In cases of significant wear, the pin can be easily replaced, reducing maintenance complexity and cost. As shown in Figure 2, the softer copper pin ensures alignment integrity, which is critical for accurate MCP torque estimation.

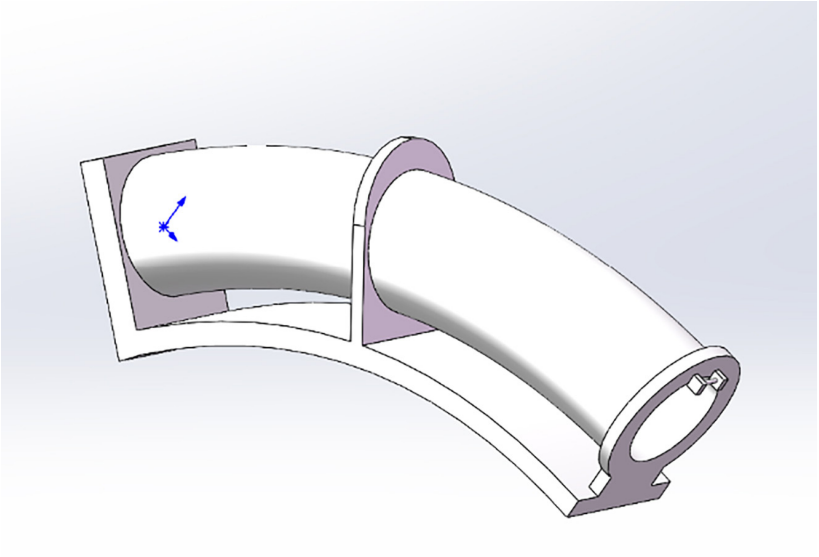

Fig. 2. Three-dimensional modelling of the thumb support block

The first joint support block secures the connection between the finger and the palm in the rehabilitation robotic arm. It attaches to the palm using bolts, while the connection to the first joint is established through copper pivot pins. The bolted interface allows easy replacement of components in case of damage or improper use, thereby protecting the main structure. Similarly, the use of copper pivot pins enables quick replacement in the event of severe wear, reducing the need to replace major parts and minimizing long-term maintenance costs. As shown in Figure 3, the bolted palm interface facilitates rapid module swapping during size adaptation tests without altering the main frame inertia used in simulation.

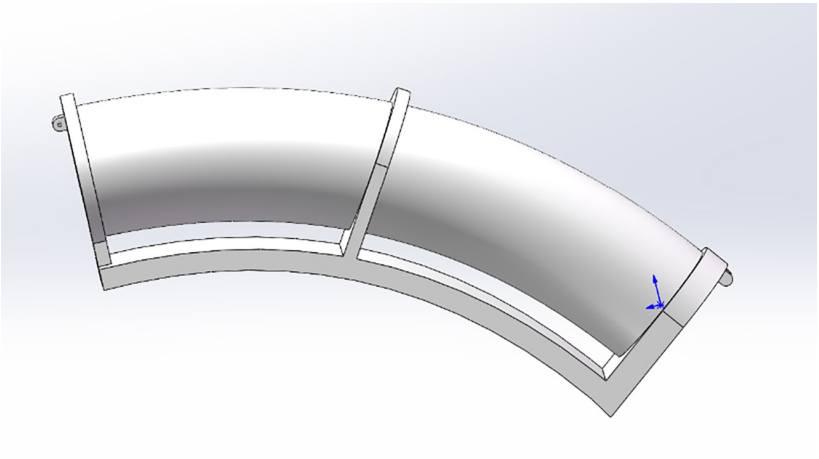

Fig. 3. Modelling of the first joint support block

The first joint serves as the primary actuation point for the electric cylinder. The cylinder's output shaft extends forward and, through a connecting rod, drives the joint to rotate about a pivot pin, simulating the flexion of the human finger's first joint. Because finger lengths vary, with the middle finger being the longest, followed by the ring, index, little finger, and thumb, the joint dimensions are adjusted accordingly. In addition to enabling motion, the first joint provides the mounting interface for the second joint. The second joint, constrained by its support block, operates in coordination with the first joint under electric cylinder actuation to replicate natural finger movement.

High-strength aluminum alloy is used for structural durability, while the joint pin incorporates an oil-free, self-lubricating copper sleeve to reduce friction, minimize wear on critical components, and lower long-term maintenance costs. Figure 4 illustrates the copper sleeve design, which reduces friction and aligns simulated torque–angle curves with experimental measurements by minimizing Coulomb offsets.

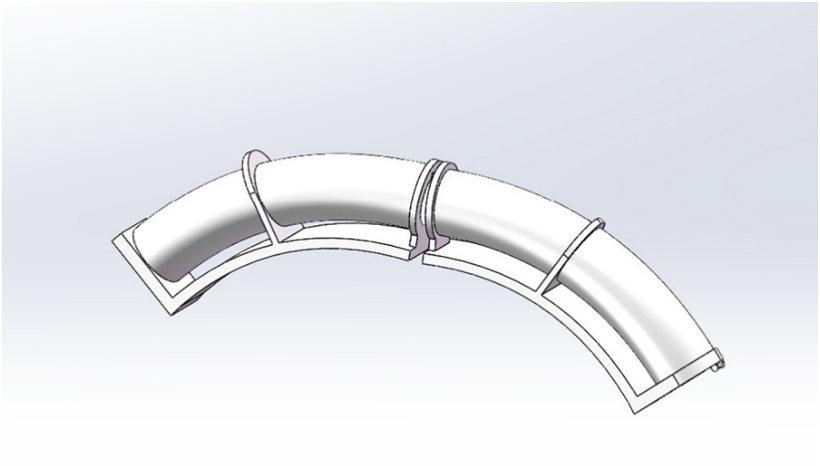

Fig. 4. CAD model of the first joint showing copper sleeve for friction reduction

The second joint fixing block connects to the first joint fixing block and secures the rotating second joint. It features an arc-shaped groove that guides the motion of the second joint pin, replicating the trajectory of the human finger's second joint. The fixing block is attached to the first joint using an arc-shaped connecting plate and bolted connections. This bolted assembly simplifies replacement and repair, reducing maintenance complexity and long-term costs. Figures 5 and 6 illustrate the arc groove that constrains the pin path, with its radius parameterized from Table 1 to accurately reproduce PIP joint kinematics.

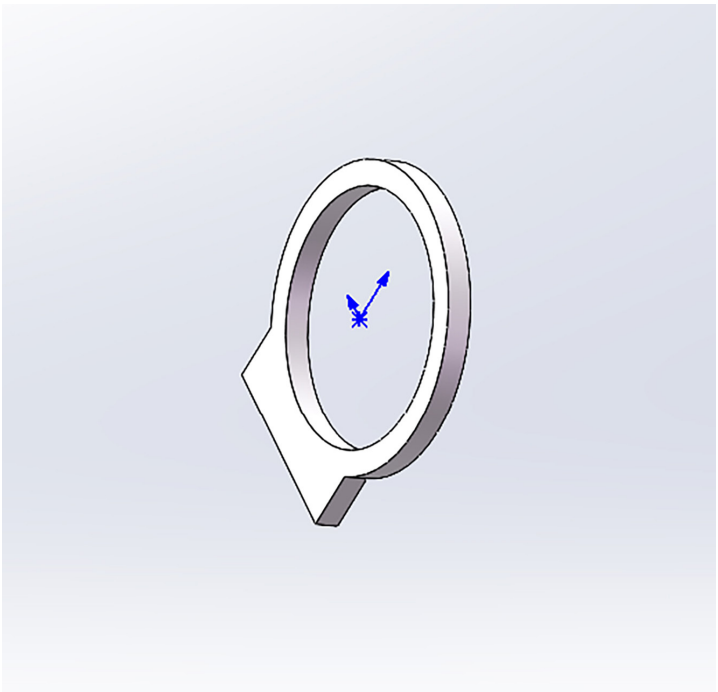

Fig. 5. Connection plate of the second joint fixing block and the first joint fixing block

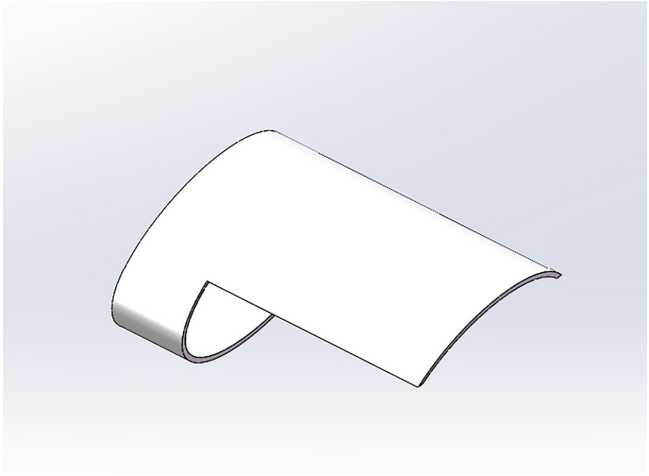

Fig. 6. Modelling of the second joint fixing block

The second joint is mounted within the second joint fixing block (see Figure 7) and replicates the motion trajectory of the distal finger joints. Its connection to the first joint is achieved through a connecting rod mechanism, while its interface with the fixing block employs a sliding constraint structure. This configuration enables the second joint to follow the required trajectory for finger flexion and extension. Because distal joint lengths vary among fingers, average dimensional parameters derived from population statistics were adopted to accommodate a wide range of patients in rehabilitation training. As shown in Figure 7, the sliding constraint within the fixing block generates the required coupler curve for DIP motion when driven by the same linear input.

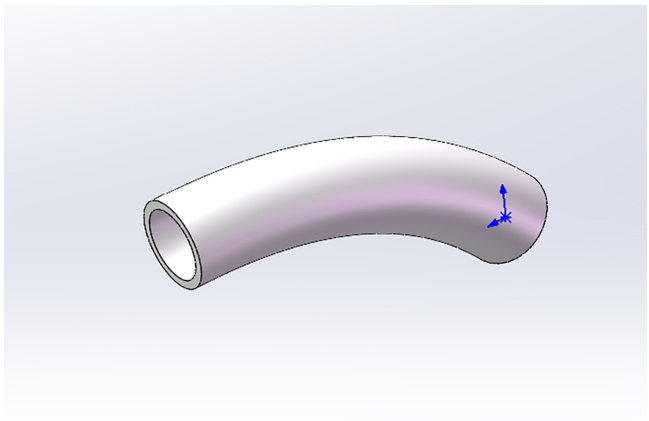

Fig. 7. Modelling of the second joint

2.4 Arm straps design and assembly

The strap secures the patient's arm and fingers to the rehabilitation device, ensuring effective transmission of therapeutic motions. Its adjustable elasticity accommodates different arm sizes and weights, providing comfort during therapy and preventing secondary injuries caused by mechanical abrasion. To enhance safety, diffuse reflective switches are integrated as interlocks: if the strap is not properly fastened, the device remains locked and cannot be activated. This feature prevents equipment damage and protects the patient from improper use. Figure 8 illustrates the integration of diffuse-reflective interlocks, where improper fastening inhibits actuation, safeguarding trials that calibrate pressure–angle maps.

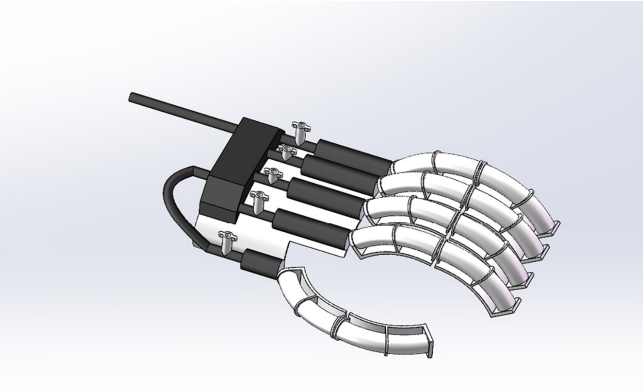

Fig. 8. Design modelling of finger and arm straps

The joints operate in coordination, interacting to replicate and analyze finger movements during common functional actions. Figure 9 shows the assembled sub-modules that collectively transmit pneumatic force to the MCP, PIP, and DIP joints, completing the six-link model used in simulation.

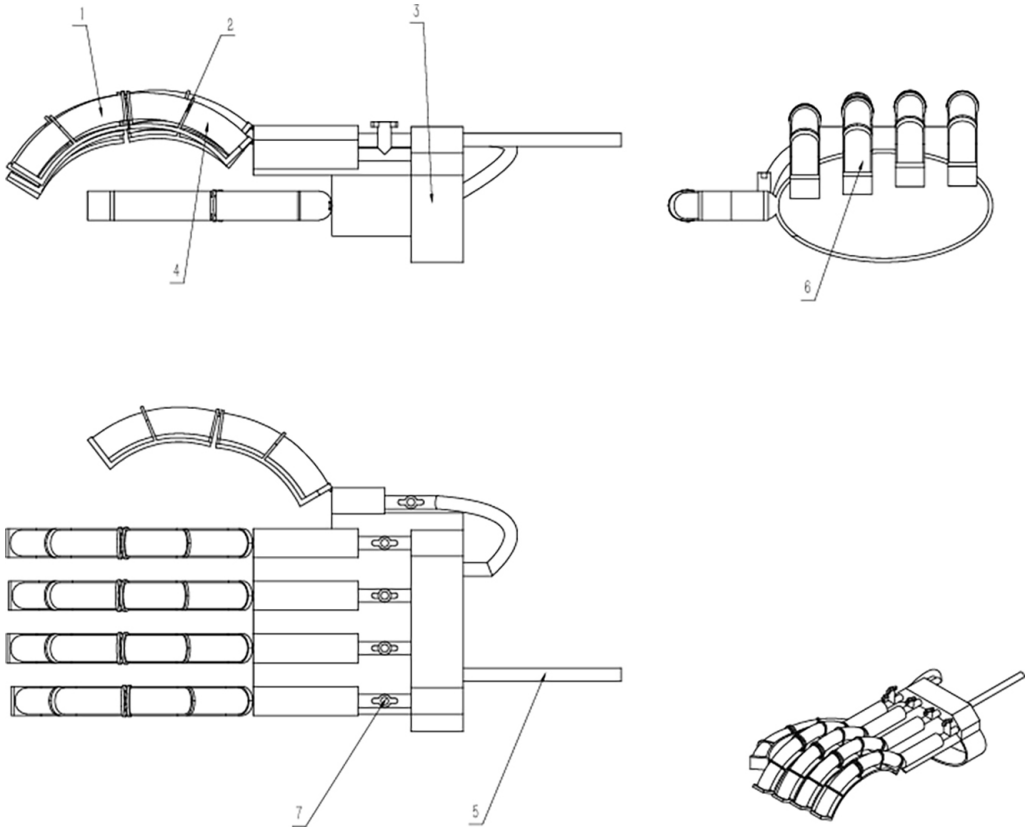

Fig. 9. Finger rehabilitation robot arm assembly

2.5 Discrete PID control with aerodynamic drag compensation

The pneumatic actuators serve as the core power source of the finger rehabilitation robot, operating on the principle of converting compressed air energy into

precise mechanical motion to drive natural finger flexion and extension. The system adopts a stage-specific pressure control strategy: compressed air is supplied at adjustable pressures (0.1 MPa for early mobilization, 0.2 MPa for intermediate training, and 0.3 MPa for intensive training) to adapt to different patient recovery phases. When air is delivered to the actuator chamber, the internal pressure rise pushes the piston to extend, and this linear motion is transmitted to the MCP, PIP, and DIP joints via a modular four-link mechanical structure to achieve bending angles of 28°, 48°, and 80°, respectively, within 2.5 seconds.

The control system under investigation is a discrete-time PID controller with aerodynamic drag compensation, designed to regulate rotational speed in a pneumatic or electromechanical actuator system. The controller operates in a sampled-data configuration with a fixed cycle time Δt, and computes control inputs in the form of actuator pressure commands u_k to achieve a desired reference speed ω_{ref}.

Aerodynamic drag is explicitly included in the model to represent realistic resistive torques encountered during high-speed operation. This ensures that the controller accounts for nonlinear disturbances arising from rotational motion in air, which is particularly relevant in biomedical devices, robotic actuators, and rehabilitation equipment.

The controller uses a standard proportional–integral–derivative (PID) algorithm, implemented in discrete-time. The discrete time PID controller computes the control input based on a delayed measurement of actuator speed to account for realistic sensor and processing dynamics. At each sampling step, the measured speed is given by:

$$\omega_k \leftarrow \text{MeasureSpeed}(t - \tau_{\text{delay}})$$

where τ_{delay} is the sensing and communication latency. The speed error is then computed as $e_k = \omega_{\text{ref}} - \omega_k$ is computed. The PID output is then calculated as:

$$u_k = K_p e_k + K_i \sum_{i=0}^{k} e_i \Delta t + K_d \frac{e_k - e_{k-1}}{\Delta t}$$

where K_p, K_i, and K_d are the proportional, integral, and derivative gains, respectively.

To prevent actuator saturation and integral windup, anti-windup logic is applied: the control signal is clamped between 0 and P_{max}, and the integral term is paused when saturation occurs. The net torque, including aerodynamic drag, is computed as

$$\tau_{\text{net}} = u_k K_\tau - T_{\text{load}} - \tau_{\text{drag}}$$

and the actuator speed is updated using

$$\omega_{k+1} = \omega_k + \frac{\tau_{\text{net}}}{J} \Delta t$$

where J is the rotational inertia of the system. The previous speed error is stored for the derivative calculation in the next cycle. The controller repeats this loop until the end of the simulation or experimental trial T_{end}.

The control algorithm is implemented in MATLAB for numerical simulations, as shown in Algorithm 1. A fixed sampling period Δt = 10 ms is used, consistent with typical actuator control rates in biomedical and robotic applications. System parameters, including actuator torque constant, drag coefficient, and load inertia, are defined as in the results section during the simulation. The methodology enables

evaluation of system performance under open-loop disturbances, the influence of aerodynamic drag, and the effectiveness of discrete-time PID control.

Algorithm 1: Discrete PID Control with Aerodynamic Drag Compensation Algorithm

Require: Target speed ω_{ref}, Supply Pressure P_{max}, Cycle time Δt, Air density ρ
Ensure: Control input u_k (Pressure)
1. **Initialize:**
   $\omega_0 \leftarrow 0$, $e_{sum} \leftarrow 0$, $e_{prev} \leftarrow 0$
2. **While** $t < T_{end}$ **do**
   2.1 **Error Calculation**
      Measure current speed: $\omega_k \leftarrow$ MeasureSpeed(t – τdelay)
      Compute error: $e_k \leftarrow \omega_{ref} - \omega_k$
   2.2 **PID Computation**
      $P_{term} \leftarrow K_p \cdot e_k$
      $I_{term} \leftarrow K_i \cdot (e_{sum} + e_k \cdot \Delta t)$
      $D_{term} \leftarrow K_d \cdot (e_k - e_{prev})/\Delta t$
      Compute control input: $u_k \leftarrow P_{term} + I_{term} + D_{term}$
   2.3 **Actuator Saturation and Anti-Windup**
      If $u_k > P_{max}$ **then**
         $u_k \leftarrow P_{max}$
         Pause integration: $e_{sum} \leftarrow e_{sum}$
      Else if $u_k < 0$
         $u_k \leftarrow 0$
         $e_{sum} \leftarrow e_{sum} + e_k \cdot \Delta t$
      End if
   2.4 **Physical Plant Update (Simulation)**
      Compute aerodynamic drag torque: $\tau_{drag} \leftarrow 0.5 \cdot C_d \cdot \rho \cdot A \cdot \omega_k^2$
      Compute net torque: $\tau_{net} \leftarrow (u_k \cdot K_\tau) - T_{load} - \tau_{drag}$
      Update speed: $\omega_{k+1} \leftarrow \omega_k + (\tau_{net}/J) \cdot \Delta t$
   2.5 **Update Previous Error:** $e_{prev} \leftarrow e_k$
   2.6 Increment step: $k \leftarrow k + 1$
3. **End while**

In the discrete-time PID control model, the actuator speed measurement incorporates a sensing delay τ_{delay} to reflect realistic sensor dynamics. At each control step, the measured speed is expressed as

$$\omega_k \leftarrow \text{MeasureSpeed}(t - \tau_{delay})$$

where ω_k is the speed used by the controller at the current time step, and τ_{delay} represents the time lag between the actual actuator speed and the available sensor reading. This delay accounts for signal processing, sensor response, and communication latency in practical implementations, and it affects the computation of the PID control action by introducing a temporal offset in the feedback loop.

3 RESULTS AND DISCUSSIONS

The numerical simulations were conducted using the discrete-time PID control model with aerodynamic drag compensation. The system was initialized with the following parameters to evaluate the actuator response under consistent operating conditions. All simulations incorporate the sensor delay τ_{delay} in the speed measurement. The system was initialized with the following parameters:

- Target speed: ω_{ref} = 2400 rpm
- Maximum supply pressure: P_{max} = 0.6 MPa

- Load torque: $T_{load} = 120$ N·m
- Control cycle: $\Delta t = 10$ ms
- Air density: $\rho = 1.225$ kg/m^3
- PID gains: $K_p = 8.5$, $K_i = 0.5$, $K_d = 1.2$
- Sensor delay: $\tau_{delay} = 5$ ms (typical measurement latency)

The constant system inputs and controller parameters were maintained to isolate the effects of intrinsic dynamics, including the influence of sensor delay, aerodynamic drag, and pressure compressibility.

3.1 Pressure–amplitude behavior

The performance of pneumatic rehabilitation manipulators is strongly influenced by supply pressure, which directly determines the angular displacement of finger joints during flexion–extension movements. To evaluate this relationship, the experimental design established a pneumatic pressure variable range of 0.1 MPa, 0.2 MPa, and 0.3 MPa while maintaining constant motor speed and load parameters. following the simulation startup, the actuator's settling time (from initiation to steady state). The resulting joint amplitudes were recorded over a 2.5-second interval, as shown in Figure 10.

The results demonstrate a positive correlation between input pressure and bending amplitude. At 0.1 MPa, the bending angle gradually increased from 0° to 28° within 2.5 seconds, providing mild mobilization suitable for early rehabilitation. At 0.2 MPa, the amplitude reached 48°, indicating intermediate training intensity. At 0.3 MPa, the joint achieved an amplitude of 80° within the same time frame, enabling large-angle movements appropriate for intensive strengthening exercises.

These findings highlight the adaptability of pneumatic actuation across different recovery phases. Low-pressure operation minimizes muscle strain and reduces the risk of injury during early rehabilitation, while higher pressures allow for more aggressive training as the patient regains strength. This behavior forms the basis of an adaptive pressure control strategy, where pneumatic actuation levels are dynamically adjusted to balance therapeutic effectiveness with patient safety.

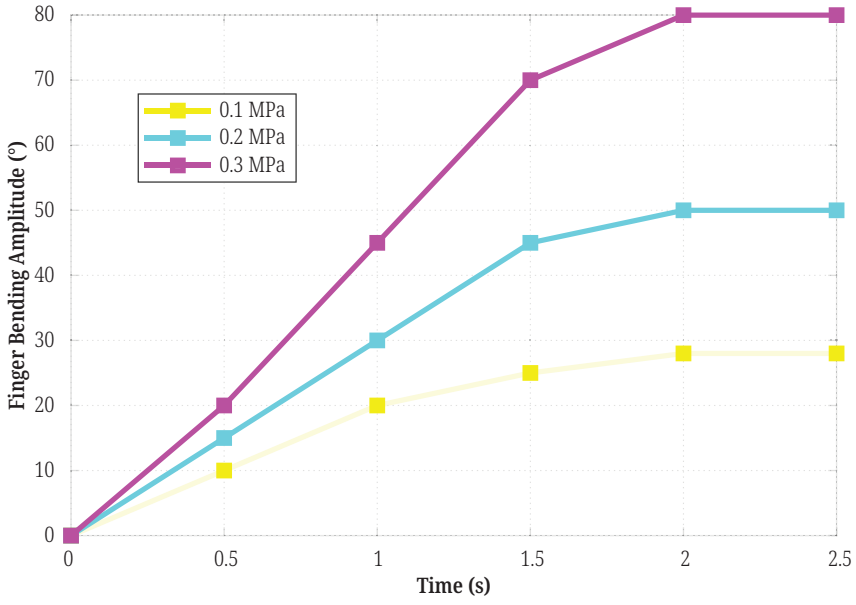

Fig. 10. Finger bending amplitude vs. time under different pneumatic pressures

3.2 Latency–performance behavior

In telerehabilitation scenarios, network latency is a critical factor influencing both responsiveness and control accuracy of pneumatic rehabilitation manipulators. To investigate the influence of communication delays in a networked control setup, simulations were conducted with varying network latency values, modeled as an additional delay τ_{net} in the speed measurement used by the PID controller shown in Algorithm 1. The effective measured speed at time step k becomes:

$$\omega_k \leftarrow \text{MeasureSpeed}(t - \tau_{delay} - \tau_{net})$$

where τ_{delay} represents sensor latency and τ_{net} represents network-induced delay. To quantify this effect, system response time and control error were evaluated under network delays ranging from 0 ms to 200 ms, as illustrated in Figures 11 and 12.

As shown in Figure 11, system response time increases approximately linearly with network latency. At 0 ms delay, the baseline response time is 2.5 s. When latency reaches 200 ms, the response time extends to 3.8 s, representing an additional 1.3 s lag. On average, every 50 ms of added latency prolongs the response time by 0.2–0.5 s. Such delays impair synchronization between patient actions and device feedback, which is essential for real-time rehabilitation.

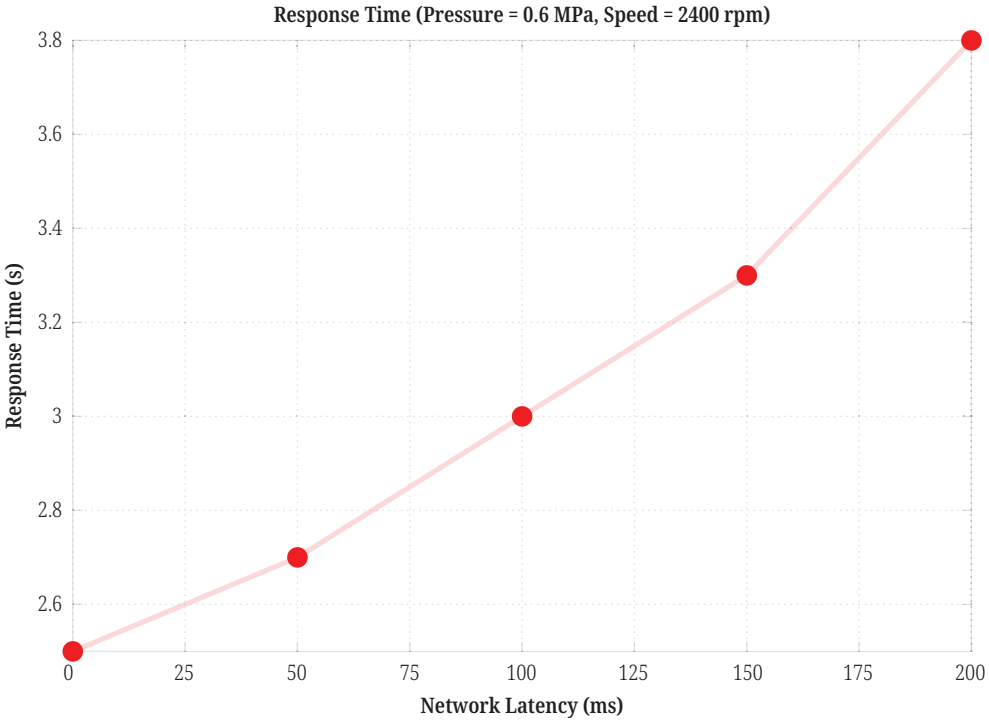

Fig. 11. Response time vs. network latency

Similarly, Figure 12 demonstrates a nonlinear relationship between latency and control error. The error rises gradually from 1.0° at 0 ms to 3.8° at 100 ms, then accelerates sharply, reaching 7.3° at 200 ms. This threshold effect indicates that system performance deteriorates significantly once latency exceeds 100 ms, increasing the risk of inaccurate joint trajectories and potential secondary injury. Collectively, these findings highlight the necessity of maintaining network latency below 50 ms to preserve near-baseline response times (~2.7 s) and limit control errors within clinically acceptable ranges (≤3.8°).

These results emphasize the importance of considering network-induced delays when designing networked or tele-operated control systems, particularly in biomedical or rehabilitation applications where timing precision and smooth motion are critical. For remote rehabilitation systems, implementing predictive control algorithms and error-compensation strategies is essential to mitigate latency effects and ensure stable, accurate performance.

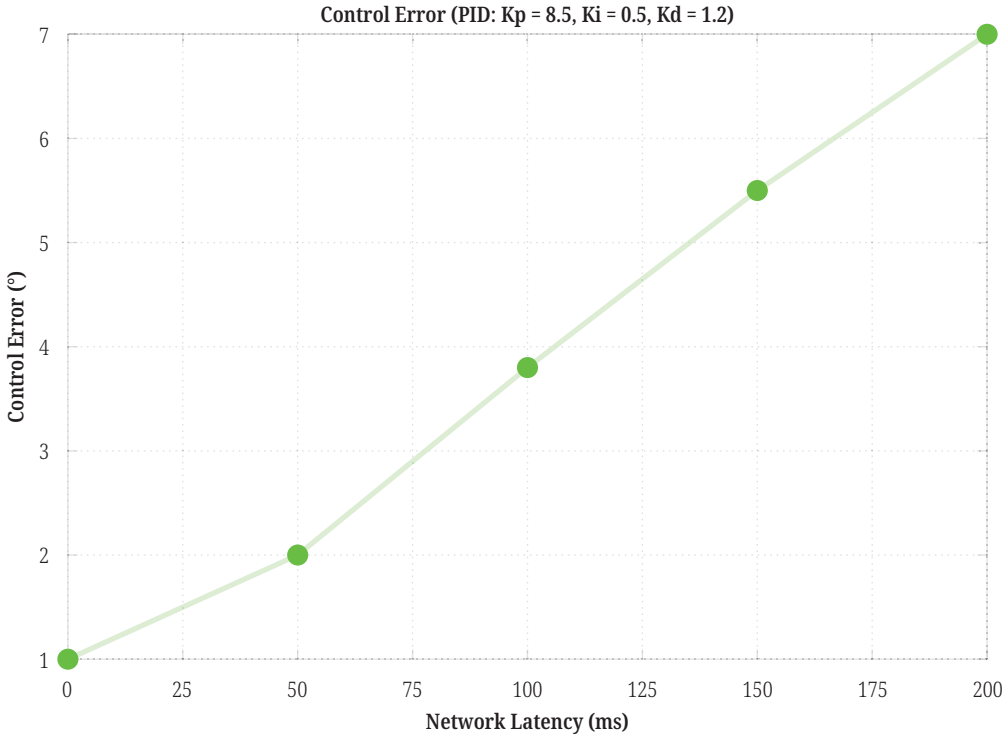

Fig. 12. Control error vs. network latency

4 CONCLUSION

This study proposes a lightweight, modular, and wearable pneumatic finger rehabilitation robot specifically designed for remote rehabilitation applications. It addresses key issues in existing systems, such as excessive complexity, limited adaptability, and poor portability. Through systematic simulations and controlled experiments, the core performance characteristics of the proposed system are validated.

The device employs a phased pneumatic actuation strategy, utilizing distinct supply pressures to achieve different functionalities, where 0.1 MPa enables gentle movement (28° flexion range), suitable for early-stage rehabilitation; 0.2 MPa supports intermediate training (48° flexion range); and 0.3 MPa enables intensive functional training (achieving 80° flexion within 2.5 seconds). This adaptive pressure control balances therapeutic efficacy and safety, establishing a progressive rehabilitation pathway. The parametric modular four-bar linkage design, based on anthropometric hand dimensions, accommodates varying finger lengths without customization, significantly enhancing adaptability to diverse patient body types. Performance evaluations under controlled network latency (0–200 milliseconds) indicate that when latency remains below 50 milliseconds, the system maintains near-benchmark responsiveness (response time approximately 2.7 seconds) while controlling angular error within 2°.

The core innovation of this study lies in its successful integration of modular mechanical design, phased pneumatic control, low-latency remote rehabilitation communication, and user-centered safety features. This synergy establishes a scalable, cost-effective personalized finger rehabilitation framework. The findings provide concrete quantitative design criteria for pressure regulation, latency management, and motion precision, advancing patient-centered rehabilitation technology.

The novel contributions of this work include:

- Modular Design: Accommodates varying finger lengths without requiring customization, improving adaptability across patient populations.
- Reduced Actuator Count: Achieves approximately 30% reduction in actuator usage compared to conventional multi-joint systems, simplifying control and lowering cost.
- Pneumatic Actuation Strategy: Implements a stage-specific pressure control (0.1 MPa for early mobilization, 0.3 MPa for intensive training), enabling safe and progressive rehabilitation.
- Tele-Rehabilitation Capability: Maintains control accuracy within 2° and latency under 50 ms, supporting real-time remote therapy.
- Simulation-Driven Validation: Combines CAD modeling and dynamic simulation to ensure mechanical fidelity and predict performance under varying conditions.
- User-Centered Safety Features: Includes diffuse reflective interlocks and self-lubricating components to enhance safety, comfort, and long-term usability.

These innovations collectively support the development of a scalable, cost-effective, and clinically viable solution for individualized finger rehabilitation. The findings establish quantitative design criteria for pressure control, latency management, and accuracy requirements, contributing to the advancement of safe, efficient, and patient-centered rehabilitation technologies.

Despite promising results, this study has several limitations. First, prototype evaluation was restricted to numerical simulations and experiments. Second, pneumatic actuation, while offering compliance and cost benefits, limits positioning accuracy compared to motor-driven systems. Third, patient variability such as differences in muscle tone, joint stiffness, and recovery speed was not fully addressed.

Future research should focus on conducting large-scale clinical trials with diverse patient groups to validate safety, usability, and therapeutic effectiveness in real-world conditions. Enhanced sensing technologies, such as EMG, optical encoders, and motion capture, should be integrated to provide precise feedback and enable adaptive control. Exploring hybrid actuation systems that combine pneumatic mechanisms with hydraulic or smart-material actuators can improve torque output and positioning accuracy. Additionally, the development of intelligent control strategies, including machine learning-based adaptive algorithms, will support personalized therapy tailored to individual patient needs. Finally, optimizing tele-rehabilitation through predictive control and latency compensation techniques is essential to ensure robust and responsive remote operation.

5 ACKNOWLEDGMENT

This work was supported by the Ministry of Higher Education under Fundamental Research Grant Scheme (FRGS/1/2024/TK07/UKM/02/14).

6 REFERENCES

[1] S. Talaa, M. El Fezazi, A. Jilbab, and M. H. El yousfi Alaoui, "Computer vision-based approach for automated monitoring and assessment of gait rehabilitation at home," *Int. J. Online Biomed. Eng.*, vol. 19, no. 18, pp. 139–157, 2023. https://doi.org/10.3991/ijoe.v19i18.43943

[2] E. Osayande, K. P. Ayodele, and M. A. Komolafe, "Development of a robotic hand orthosis for stroke patient rehabilitation," *Int. J. Online Biomed. Eng.*, vol. 16, no. 13, pp. 142–149, 2020. https://doi.org/10.3991/ijoe.v16i13.13407

[3] A. Arabiat, M. Matahen, O. Abu Zaid, and M. Zgoul, "Control of an exoskeleton for lower limb rehabilitation using ANFIS," *Int. J. Online Biomed. Eng.*, vol. 18, no. 15, pp. 122–140, 2022. https://doi.org/10.3991/ijoe.v18i15.33805

[4] B. Brahmi, "Nonlinear control of an exoskeleton seven degrees of freedom robot to realize an active and passive rehabilitation tasks," Thèse de doctorat électronique, Montréal, École de technologie supérieure, 2019.

[5] Y. Zhigang, "Research progress in rehabilitation robots," in *Proceedings of the 2019 International Conference on Robotics, Intelligent Control and Artificial Intelligence*, 2019. https://doi.org/10.1145/3366194.3366320

[6] M. R. Islam, M. Assad-Uz-Zaman, B. Brahmi, Y. Bouteraa, I. Wang, and M. H. Rahman, "Design and development of an upper limb rehabilitative robot with dual functionality," *Micromachines (Basel)*, vol. 12, no. 8, p. 870, 2021. https://doi.org/10.3390/mi12080870

[7] Q. Liu, S. Ghodrat, and K. M. B. Jansen, "Design and modelling of a reversible shape memory alloy torsion hinge actuator," *Mater. Des.*, vol. 237, p. 112590, 2024. https://doi.org/10.1016/j.matdes.2023.112590

[8] L. Wang, P. Xu, J. Li, S. Ekaterina, and B. Wang, "Stability analysis of human hand grasping for the design of pneumatic muscle-driven end effector targeting citrus picking," *Comput. Electron. Agric.*, vol. 239, p. 110942, 2025. https://doi.org/10.1016/j.compag.2025.110942

[9] Y. Yan, X. Chen, C. Cheng, and Y. Wang, "Design, kinematic modeling and evaluation of a novel soft prosthetic hand with abduction joints," *Med. Nov. Technol. Devices*, vol. 15, p. 100151, 2022. https://doi.org/10.1016/j.medntd.2022.100151

[10] Y. Tian *et al.*, "Mechanical design and analysis of the end-effector finger rehabilitation robot (EFRR) for stroke patients," *Machines*, vol. 9, no. 6, p. 110, 2021. https://doi.org/10.3390/machines9060110

[11] S. Martiñón and R. Hernández-Miramontes, "Use of exoskeletons in the treatment and rehabilitation of paraplegia patients," in *Paraplegia*, 2021. https://doi.org/10.5772/intechopen.94920

[12] A. W. Heinemann *et al.*, "Experience of robotic exoskeleton use at four spinal cord injury model systems centers," *J. Neurol. Phys. Ther.*, vol. 42, no. 4, pp. 256–267, 2018. https://doi.org/10.1097/NPT.0000000000000235

[13] R. Charbonneau, A. Loyola-Sanchez, K. McIntosh, G. MacKean, and C. Ho, "Exoskeleton use in acute rehabilitation post spinal cord injury: A qualitative study exploring patients' experiences," *J. Spinal Cord Med.*, vol. 45, no. 6, pp. 848–856, 2022. https://doi.org/10.1080/10790268.2021.1983314

[14] N. Postol, N. J. Spratt, A. Bivard, and J. Marquez, "Physiotherapy using a free-standing robotic exoskeleton for patients with spinal cord injury: A feasibility study," *J. Neuroeng. Rehabil.*, vol. 18, no. 1, p. 180, 2021. https://doi.org/10.1186/s12984-021-00967-4

[15] L. Zhao *et al.*, "A novel underactuated exoskeleton rehabilitation glove for hand flexion and extension training," *Biomimetic Intelligence and Robotics*, vol. 5, no. 4, p. 100248, 2025. https://doi.org/10.1016/j.birob.2025.100248

[16] D. Y.-L. Lim, H.-S. Lai, and R. C.-H. Yeow, "A bidirectional fabric-based soft robotic glove for hand function assistance in patients with chronic stroke," *J. Neuroeng. Rehabil.*, vol. 20, no. 1, p. 120, 2023. https://doi.org/10.1186/s12984-023-01250-4

[17] J. Wang and Y. Fei, "Design and modelling of flex-rigid soft robot for flipping locomotion," *J. Intell. Robot. Syst.*, vol. 95, no. 2, pp. 379–388, 2019. https://doi.org/10.1007/s10846-018-0957-7

[18] S. Corbianco *et al.*, "Energy cost and psychological impact of robotic-assisted gait training in people with spinal cord injury: Effect of two different types of devices," *Neurol. Sci.*, vol. 42, no. 8, pp. 3357–3366, 2021. https://doi.org/10.1007/s10072-020-04954-w

[19] D. J. Edwards *et al.*, "Walking improvement in chronic incomplete spinal cord injury with exoskeleton robotic training (WISE): A randomized controlled trial," *Spinal Cord*, vol. 60, no. 6, pp. 522–532, 2022. https://doi.org/10.1038/s41393-022-00751-8

[20] A. Echemendía Del Valle *et al.*, "Effects of a gait training program on spinal cord injury patients: A single-group prospective cohort study," *J. Clin. Med.*, vol. 12, no. 23, p. 7208, 2023. https://doi.org/10.3390/jcm12237208

[21] S. H. Yoo, M. Kim, H. J. Park, G. I. Lee, S. H. Lee, and M. K. Kwak, "Vacuum-powered soft actuator with oblique air chambers for easy detachment of artificial dry adhesive by coupled contraction and twisting," *Sci. Technol. Adv. Mater.*, vol. 24, no. 1, p. 2274818, 2023. https://doi.org/10.1080/14686996.2023.2274818

[22] W. Li, D. Hu, and L. Yang, "Actuation mechanisms and applications for soft robots: A comprehensive review," *Appl. Sci. (Basel)*, vol. 13, no. 16, p. 9255, 2023. https://doi.org/10.3390/app13169255

[23] B. Xia, J. Fu, H. Zhu, Z. Song, Y. Jiang, and H. Lipson, "A legged soft robot platform for dynamic locomotion," in *2021 IEEE International Conference on Robotics and Automation (ICRA)*, 2021, pp. 11812–11819. https://doi.org/10.1109/ICRA48506.2021.9561018

[24] K. Park, J. Ha, B. Shin, and H.-Y. Kim, "Chapter 7. Hygroresponsive movements of plants and soft actuators," in *Soft Matter Series*, Cambridge: Royal Society of Chemistry, 2022, pp. 227–240. https://doi.org/10.1039/9781839161162-00227

7 AUTHORS

Dongze Li is currently an M.Sc. student in the Department of Electrical, Electronic & System Engineering, Universiti Kebangsaan Malaysia. He is currently working on a project related to the development of a robotic arm and system in a healthcare application. His research interest is numerical simulation, 3D modeling and embedded system development (E-mail: p123122@siswa.ukm.edu.my).

Kok Beng Gan has received the B.S. degree in Material Physics from University Technology Malaysia in 2001. He was conferred a PhD (Electrical, Electronic & System Engineering) from Universiti Kebangsaan Malaysia in 2009. He was an engineer in the field of electronic manufacturing services and original design manufacturing from 2001 to 2005. After several years of industry experience, he decided to venture into academia in 2005. He is currently an Associate Professor in the Department of Electrical, Electronic & Systems Engineering, Faculty of Engineering and Built Environment, Universiti Kebangsaan Malaysia. He specializes in embedded systems and artificial intelligence. His current research interest is artificial intelligence in healthcare, embedded systems & signal processing for medical & industry applications, and biomechanics & human motion analysis (E-mail: kbgan@ukm.edu.my).

Kok Swee Sim is currently a Professor with Multimedia University, Malaysia. He actively collaborates with various local and international universities

and hospitals. He has filed 23 patents and 85 software copyrights. He is a fellow of the Academy of Sciences Malaysia, the Institution of Engineers Malaysia (IEM), and the Institution of Engineering and Technology (IET), U.K. Over the years, he has received numerous prestigious national and international awards. These include the Japan Society for the Promotion of Science (JSPS) Fellowship in 2018; the Top Research Scientists Malaysia (TRSM) Award from the Academy of Sciences Malaysia in 2014; and Korean Innovation and Special Awards in 2013, 2014, and 2015. He was a recipient of the TM Kristal Award and multiple World Summit on the Information Society (WSIS) Prizes in 2017, 2018, 2019, 2020, and 2021 (E-mail: kssim@mmu.edu.my).